Springer

KSME

Journal of Mechanical Science and Technology 24 (7) (2010) 1401~1410
www.springerlink.com/content/1738-494x
DOI 10.1007/s12206-010-0412-6

Molecular dynamics study on the effect of solution-wall interaction potential on the properties of solution in uniformly charged hydrophobic channel †

Hai Hoang, Sangmo Kang and Yong Kweon Suh*

Department of Mechanical Engineering, Dong-A University, Saha-gu, Busan, 604-714, Korea

(Manuscript Received June 19, 2009; Revised January 28, 2010; Accepted March 4, 2010)

Abstract

We numerically investigate the effect of the solution-wall (i.e., water-wall and ion-wall) interaction potential on the properties of confined aqueous solution by using molecular dynamics (MD) simulations. The effect is determined by comparing results obtained from the MD simulation using the Lennard-Jones (L-J) potential for the water-wall and ion-wall interactions and those using a purely repulsive potential, i.e., the Weeks-Chandler-Andersen-like potential. In the MD simulations, 680 water molecules and 20 chloride ions are included between uniformly charged plates that are separated by 2.6 nm. The results show that the properties of solution are influenced only in the region close to the wall: The water molecules are more densely packed for the case of the L-J potential. Comparison of the results of the MD simulations in the case of the L-J potential with those provided by solving the Poisson-Boltzmann equation, we found that classical continuum theory fails to predict the ion density and electrostatic potential distributions in the region near to the wall, but far way from the wall, the prediction from the continuum theory is in line with the MD simulation.

Keywords: Molecular dynamics simulation; Aqueous solution; Hydrophobic plate; WCA potential; PPPM methods

1. Introduction

Understanding the interfacial phenomena concerning solution in contact with a surface, e.g., the electrical double layer (EDL) and electrokinetic transport, plays an important role in biological and chemical science. Over the recent years, some studies have been performed with molecular dynamics (MD) simulations in which the interfacial phenomena are numerically investigated in terms of the effect of various factors such as the characteristics of the surface, i.e., hydrophobic and hydrophilic behaviors and ion specificity, etc. [1-5]. One of the important conclusions obtained from these studies is that the fluid-wall interaction has a significant effect on the interfacial phenomena. In these studies, the fluid-wall interaction is modeled by the well-known 12-6 Lennard-Jones (L-J) potential, which is composed of two parts, the attractive and repulsive parts. As mentioned in Bocquet's series studies [1-3], a proper knowledge on the contribution of each part to the phenomena of the fluid also plays an important role in the biological and chemical science. To evaluate the effect of the attractive part of the potential, we can tune the coefficient c_{ij} given in Bocquet's studies [1-3]. Alternatively, we can also use the Weeks-Chandler-Andersen (WCA) potential which is a modification of the 12-6 L-J potential such that only the repulsive force should act [6-8]. Hence we can examine indirectly the role of the attractive part of the L-J potential for the static and dynamic properties of the liquid by comparing the results obtained by the L-J potential with those by the WCA potential. Travis *et al*. [8] performed MD simulations for Poiseuille flow of L-J fluid in narrow slit pores by using both the L-J and WCA potentials for liquid-liquid, liquid-solid and solid-solid interactions. They found that the liquid structures and velocity profiles depend on the potential model employed, which implies that the attractive part of the fluid-wall interaction potential has a significant effect on the properties of the fluid.

In fact, the fluid-wall interaction can be modeled by another functional form of the L-J potential, e.g. the 9-3 L-J potential [9-14]. This potential is generally used to represent the interaction between the fluid molecule and the hydrophobic homogeneous wall. In this work, we also use the 9-3 L-J potential for the fluid-wall interaction. Similar to the case with the 12-6 L-J potential, the effect of the attractive part of the 9-3 L-J potential can be investigated by comparing the results obtained by the 9-3 L-J potential and those by a Weeks-Chandler-Andersen-like (WCAL) repulsive potential which is intrinsically the same as the WCA potential [9]. To investigate the effect of water-wall interaction potential on the properties of confined water, Kumar *et al*. [9] conducted an MD simula-

† This paper was recommended for publication in revised form by Associate Editor Do Hyung Lee

*Corresponding author. Tel.: +82 51 200 7648, Fax: +82 51 200 7656
E-mail address: yksuh@dau.ac.kr

tion for the water confined in the non-charged nano-channel by using the 9-3 L-J and WCAL repulsive potentials for liquid-solid interaction. They found that the properties of liquid are weakly dependent on the kinds of potentials for the specific case of smooth walls.

As summarized above, the role of the repulsive part of the fluid-wall interaction potential has been addressed in a few papers. We see that depending on the specific problem the attractive part of the fluid-wall interaction potential may affect the properties of the liquid. Further, no studies have been reported so far which consider the influence of the attractive part of the potential on the ions, water concentrations, polarization of water, and diffusion of water, etc., for the aqueous solution confined between uniformly charged hydrophobic plates.

In this paper, we used the MD method to study the effect of the water-wall and ion-wall interaction potentials on the properties of chloride solutions confined between uniformly charged smooth plates. We compared the results obtained by using the WCAL potential with those by the L-J potential. We are also interested in comparing our results with those provided by solving the Poisson-Boltzmann equation in order to check the validity of the continuum theory in the present case.

The rest of this paper is organized as follows. In Section 2, we introduce briefly the classical theory of the EDL. The details of molecular models and potential models and MD simulations are presented in Section 3. We provide the results of the MD simulations and discussions in Section 4. Finally, the conclusions of our study are summarized in Section 5.

2. Continuum model of EDL

Under the assumption of continuum, the EDL can be described by the PB equation, which is a combination of the Poisson equation for the electrostatic potential and the Boltzmann distribution for the ion density:

$$\tilde{\varepsilon}\nabla^2\psi = -\rho_E \tag{1}$$

$$\rho_E = \sum_{i=1}^{N} \overline{z}_i e n_i \tag{2}$$

$$n_i = n_{\infty,i} \exp\left(-\frac{\overline{z}_i e\psi}{k_B T}\right) \tag{3}$$

where ψ is the local electrostatic potential, ρ_E the local charge density, e the electron charge, $\tilde{\varepsilon}$ the permittivity of the fluid, T the fluid temperature, k_B the Boltzmann constant, N the number of ion species, n_i the local number density, $n_{\infty,i}$ the number density at the channel center where the electrostatic potential is assumed to be zero and $\overline{z}_i$ the valency.

The one-dimensional PB equation in terms of the coordinate z normal to the channel wall (its origin is at the channel center, see Fig. 1) is then

$$\frac{d^2\psi}{dz^2} = -\frac{e}{\tilde{\varepsilon}} \sum_{i=1}^{N} \overline{z}_i n_{\infty,i} \exp\left(-\frac{\overline{z}_i e\psi}{k_B T}\right) \tag{4}$$

To be more convenient in the comparison of results of the continuum model and those of the MD simulation, we used only one kind of ion species, which have charges opposite to the wall charge to keep the system electro-neutral. Thus we can rewrite Eq. (4) as follows:

$$\frac{d^2\psi}{dz^2} = -\frac{e}{\tilde{\varepsilon}} \overline{z}\, n_\infty \exp\left(-\frac{\overline{z}\, e\psi}{k_B T}\right) \tag{5}$$

where $\overline{z}$ is the valency of the ion.

Boundary conditions are:

$$\frac{d\psi}{dz} = 0 \ \text{ and } \ \psi = 0 \ \ \text{at } z = z_c \tag{6}$$

where z_c is the z coordinate of the channel center; $z_c = 0$ in this study.

Integrating Eq. (5), we obtain the analytical solution:

$$\frac{d\psi}{dz} = \sqrt{\frac{2k_B T n_\infty}{\tilde{\varepsilon}}} \left[\exp\left(-\frac{\overline{z} e\psi}{k_B T}\right) - 1\right]^{1/2} \tag{7}$$

$$\psi = \frac{k_B T}{\overline{z}_0 e} \ln\left[\cos^2\left(\sqrt{\frac{n_\infty e^2 \overline{z}^2}{2\tilde{\varepsilon} k_B T}}\,(z - z_c)\right)\right] \tag{8}$$

$$n = n_\infty \exp\left(-\frac{e\overline{z}\psi}{k_B T}\right) = n_\infty \frac{1}{\cos^2\left[\sqrt{\frac{n_\infty e^2 \overline{z}^2}{2\tilde{\varepsilon} k_B T}}\,(z - z_c)\right]} \tag{9}$$

In fact, Eq. (8) has been used by Freund [15] and Kim and Darve [16]. On the MD simulation, we specify the surface charge density, σ_S, instead of n_∞. So, we must relate n_∞ to σ_S. We begin with the relation of σ_S and ψ:

$$\sigma_S = \tilde{\varepsilon} \frac{d\psi}{dz}(z = z_{wall}) \tag{10}$$

Substituting Eqs. (7) and (8) into Eq. (10), we derive the equation for the unknown value n_∞ as follows:

$$\sqrt{\frac{2n_\infty k_B T}{\tilde{\varepsilon}}} \left[\frac{1}{\cos^2\left[\sqrt{\frac{n_\infty e^2 \overline{z}_0^2}{2\tilde{\varepsilon} k_B T}}\,(z_{wall} - z_c)\right]} - 1\right]^{1/2} = \frac{\sigma_s}{\tilde{\varepsilon}} \tag{11}$$

The unknown value n_∞ is determined by numerically solving this equation by using Newton-Raphson method [17].

In the above computations, we assumed the permittivity $\tilde{\varepsilon}$ to be constant. In fact, a recent numerical study reported that the permittivity of water is appreciably varied in the vicinity of the wall [16]. However, Freund [15] reported that the influence of permittivity variation in the channel on the ion distri-

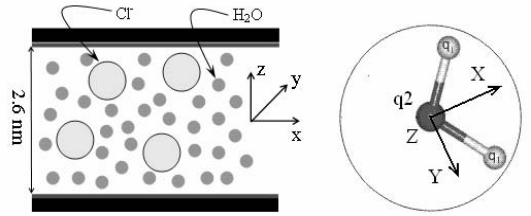

(a) (b)

Fig. 1. (a) Schematic of a nano-channel containing water molecules and ions; the inner surfaces of walls are uniformly charged; (b) SPC/E model for the water molecule and body-fixed coordinates attached to it.

bution is less important compared to the ion-wall interaction.

3. Molecular dynamics simulation

3.1 Physical and mathematical models

We performed MD simulations of a system composed of 680 water molecules and 20 chloride ions confined between two uniformly charged plates. We need a trial-and-error method to determine the number of water molecules. The basic principle is that we want to attain a desired density of water in the bulk of the channel (i.e., in the region close to the channel center) after the water molecules are adsorbed near the wall. We determine the first trial by assuming that no adsorption occurs and water molecules are uniformly distributed over the CFD domain of the channel. We simulate MD, and calculate from the result the density of the water molecules in the bulk. Then we adjust the number of molecules (we add more molecules if the density is less than the desired value, and vice versa). We repeat this process several times until the desired density is obtained with a reasonable accuracy.

Fig. 1 shows a schematic of the channel configuration subjected to the MD simulations. The SPC/E (simple point charge/ extended) model was used to model the water molecules [18]. It is a three-site model: two sites for hydrogen atoms and one site for oxygen atom [Fig. 1(b)]. In the SPC/E model, both the charge and mass are positioned at each site of the model. The O-H distance is fixed at 0.1nm and H-O-H angle at 109.47°. The point charges on the oxygen and hydrogen positions are -0.847*e* and +0.425*e*, respectively. The ions are modeled by the charged L-J particle model; a detailed description of this model will be given in the next subsection. The channel walls are composed of smooth hydrophobic plates, which are assumed to be uniformly charged on the inner surfaces with σ_s = +0.156C/m^2 in order to make the net charge electro-neutral.

In MD simulations, a water molecule is considered to be a rigid body, i.e., its motion is decomposed into two completely independent parts, the translational motion and rotation about the center of mass. The Euler angles are used to specify the orientation of the water molecules. The ion motion is described only by translation. Newton's equations governing the translational and rotational motions are [19, 20]:

Table 1. Parameters for the Lennard-Jones potential used in the simulation.

Interaction	ε (kJ/mol)	σ (nm)
O-O	0.645	0.317
O-Wall	1.250	0.250
O-Cl	0.536	0.381
Cl-Cl	0.445	0.445
Cl-Wall	1.250	0.250

$$m_i \frac{d}{dt}\mathbf{v}_i = \mathbf{F}_i \tag{12}$$

$$\frac{d}{dt}\mathbf{I}^s = \boldsymbol{\tau}^s \tag{13}$$

where, m_i is mass of the molecule (hereinafter by 'molecule' we mean the water molecule and also the chloride ion), $\mathbf{v}_i$ the velocity, $\mathbf{I}^s$ the angular momentum and $\boldsymbol{\tau}^s$ the torque about the center of mass of the molecule in the space-fixed frame. Further, for the purpose of numerical stability, we used a quaternion of a set of four scalar quantities related to the Euler angles to describe the motion of the rigid water molecules [19-20]. $\mathbf{F}_i$ is the total force exerted on the molecule; e.g., for the water molecule $\mathbf{F}_i$ is the summation of the local forces acting on two hydrogen atoms and one oxygen atom. The local force exerted on an atom *i* is the spatial gradient of the potential that consists of the L-J and electrostatic-interaction potentials between it and other atoms in the solution as well as the charged walls. The potential of the atom *i* , U_i , is given as:

$$U_i = \sum_{\mathbf{n}\in Z^2}\sum_j{}^{*}\left[\varepsilon_{ij}\left\{\left(\frac{\sigma_{ij}}{s_{ij}}\right)^{12}-\left(\frac{\sigma_{ij}}{s_{ij}}\right)^{6}\right\}+\frac{q_i q_j}{s_{ij}}\right]+ \sum_{lower-wall}^{upper-wall}\left[\int_{\infty}\frac{q_i\sigma_s dxdy}{\sqrt{(x_i-x)^2+(y_i-y)^2+(z_i-z_{wall})^2}} +U_{L-J,i}^{wall}\right] \tag{14}$$

where σ_{ij} and ε_{ij} are the L-J diameter and the L-J interaction strength for the interaction between i^{th} atom and j^{th} atom, respectively. We also have $\mathbf{s}_{ij}=\mathbf{r}_{ij}+n_x L_x\mathbf{e}_x+n_y L_y\mathbf{e}_y$, $\mathbf{r}_{ij}=\mathbf{r}_i-\mathbf{r}_j$ with $\mathbf{r}_i=(x_i,y_i,z_i)$ and $s_{ij}=|\mathbf{s}_{ij}|$. Further, $\mathbf{e}_x$ and $\mathbf{e}_y$ are unit vectors, $\mathbf{n}=(n_x,n_y)$ is a pair of integers, and L_x and L_y denote the spatial size of the physical domain. Here the superscript * indicates the omission of the term with $i=j$ when $\mathbf{n}=0$. $U_{L-J,i}^{wall}$ is the L-J potential between the i^{th} atom and the wall. In this study, we employed the 9-3 L-J potential, which is given as [9-14]:

$$U_{L-J,i}^{wall}(\tilde{z}_i)=4\varepsilon_w\left(\left(\frac{\sigma_w}{\tilde{z}_i}\right)^9-\left(\frac{\sigma_w}{\tilde{z}_i}\right)^3\right) \tag{15}$$

where $\tilde{z}_i$ is distance between the atom and a wall: $\tilde{z}_i=|z_i-z_{wall}|$. It is immediately seen that the 9-3 L-J poten-

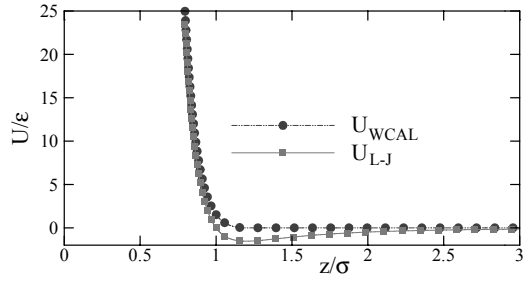

Fig. 2. The 9-3 L-J and WCAL potentials for the oxygen-wall and ion-wall interactions as a function of the position (*z*-coordinate).

tial reaches the minimum value $-8/3^{3/2}\varepsilon_w$ at $\tilde{z}_i = 3^{1/6}\sigma_w$. Table 1 summarizes the parameters of the L-J potential used in the present study [13, 21].

To test the effect of the solution-wall interaction potential on the static and dynamic properties of the solution, we also performed the MD simulation in which the L-J potential $U_{L-J,i}^{wall}$ of Eq. (15) for the solution-wall interaction is replaced by the WCAL repulsive potential that is designed by excluding the attractive part from $U_{L-J,i}^{wall}$ of Eq. (15) (see Fig. 2) as follows [9]:

$$U_{WCAL,i}^{wall}(\tilde{z}_i) = \begin{cases} 4\varepsilon_w\left[\left(\frac{\sigma_w}{\tilde{z}_i}\right)^9 - \left(\frac{\sigma_w}{\tilde{z}_i}\right)^3\right] + \frac{8}{3^{3/2}}\varepsilon_w & \text{if } \tilde{z}_i < 3^{1/6}\sigma_w \\ 0 & \text{if } \tilde{z}_i > 3^{1/6}\sigma_w \end{cases} \quad (16)$$

3.2 Numerical methods

In computing the electric force and potential for the charged atom (the 2nd and 3rd terms in Eq. (14)) in the systems with slab geometry, the EW3DC (three-dimensional Ewald summation with the correction term) is in general the most useful [22]. However, the EW3DC cannot be applicable to the present model, because the walls are assumed to be continuously charged. This problem can be overcome by using Yeh *et al.*'s modification [22] and the equivalent model of the parallel plate capacitor given by Yang *et al* [23]. We used the minimum-image criterion, cut-off and neighbor algorithms in order to effectively compute the L-J and real-space forces with cut-off radius for the L-J force equal to 0.8 nm and that for the real-space force 1.1 nm [19-21]. The PPPM (particle-particle-particle-mesh) [24] method is used for effectively computing the reciprocal-space force on the charged atoms. In this method, an FFT grid spacing of 0.1nm and a TSC (triangular shaped cloud, 2nd order) for the charge distribution and the force interpolation were chosen.

The leap-frog Verlet algorithm was used to integrate the equations of motions with the numerical time step of 1.0 fs. To avoid viscous heating, the Berendsen thermostat was used with the time constant 0.05 ps [19].

Before starting the MD simulation, the initial positions, orientation, translational and rotational velocities of all the molecules have to be assigned [25]. Since we used the Euler angles combined with quaternion coordinates to describe the motion of rigid water molecules, we must pay attention to setting the initial positions and orientations of molecules such that the intermolecular force and the torque should not be so large. To assign the initial positions and orientations of molecules satisfying these requirements, we followed a two-step treatment [25]. In the first step, all molecules were assigned with random positions and orientations, and then we performed the (potential) energy minimization to find positions of molecules in which sum of all the forces acting on the specific molecule becomes approximately zero; the orientation of the water molecules is kept constant during the process of energy minimization. The steepest descent method combined with the conjugate gradient method was applied in this energy minimization [17]. To implement the line minimization, we used the Brent method and parabolic interpolation with the spatial step size for the line search 0.01nm [17]. After this first step, we can get a configuration with small interaction force, but the interaction torque can be large. So, we need to reduce the magnitude of torque in the second step for the initial configuration. For this, we added damping terms $-\alpha_F \mathbf{v}_i$ and $-\alpha_R \mathbf{I}^s$ to the RHS of the Newton's equations (12) and (13), respectively, and numerically integrated the equations as well as the equations for the positions and angles of the molecules, see Suh *et al* [25]. In our study, we chose the damping coefficients as α_F = 0.732 N·ps/m and α_R = 12.8 ps^{-1}. We set zero for the initial values of the velocities of the molecules in the integration [25].

After the initial positions and orientations of all the molecules are assigned, their initial translational and rotational velocities must be specified. The translational velocity of each molecule is first assigned randomly from a Gaussian distribution, which then is corrected so that no overall linear momentum is produced. Finally, the magnitude of the velocities may be adjusted in such a way that the system conforms to the required temperature 300K. We specify the initial rotational velocities for each water molecule in a similar way. We first assigned their values randomly and then corrected them so that there was no overall angular momentum, and finally adjusted them to satisfy again the temperature requirement, i.e., 300K [19, 20, 25].

Now, all the preliminary set-up was completed for the main computation. To attain the equilibration in the main computation, the system was simulated for the time duration 0.5 ns (500,000 time steps). After the system reached the equilibration, we performed sampling every 10 fs for the time duration of 1.5 ns in order to compute the average statistics except for the velocity autocorrelation functions (VACF). For the VACF, the sampling was also performed every 10 fs, but data were collected only for 50 ps because of the computer memory limit. To compute distributions of the values such as density and polarization, etc., across the channel, the calculation domain was uniformly divided into x-y plane bins having the width $\Delta z = 0.029$ nm, and then the values in a bin were de-

termined by taking the average over the bin. To remove the statistical noise, the noise reduction method was used in our post production [26].

4. Results and discussions

The MD simulations were performed by developing FORTRAN code. We present the numerical results in the following sequence: In Subsection A, we provide the density profiles of oxygen, chloride ions and the electrostatic potential distribution. In addition, we compare the results given from the MD simulations with those obtained by the P-B equation. The radial distribution functions for pairs of species are provided in Subsection B. The profiles of dipolar direction of water molecules across the channel are presented in Subsection C. Finally, we address the velocity autocorrelation function for both translational and rotational motions and the diffusion coefficient in Subsection D.

4.1 Density profiles of oxygen, ion and electrostatic potential distribution

The number density of an atom species across the channel is defined as:

$$\rho(z_n) = \frac{1}{A\Delta z}\left\langle \sum_{i=1}^{N} H_n(z_i) \right\rangle \tag{17}$$

where

$$H_n(z_i) = \begin{cases} 1 \text{ if } (n-1)\Delta z \prec z_i \prec n\Delta z \\ 0 \text{ else} \end{cases} \tag{18}$$

N is the number of particles, A is the area of horizontal section of the domain, $A = L_x \times L_y$, and <.> denotes the ensemble average over M samples. Fig. 3 shows the number density of oxygen atom across the channel for both the WCAL and L-J potentials. Note that in the SPC/E model for the water molecule, the mass of the hydrogen atom is negligible compared with that of the oxygen atom (the mass ratio 1:9) and the distance between the hydrogen atom and the oxygen atom is small (1 A^0), so the center of mass of the water molecule is very close to that of the oxygen atom. This implies that the oxygen density profile is representative of the water density profile [16] (hereinafter we identify the oxygen density profile with the water density profile). We see from Fig. 3 that density profiles for both potentials are similar to each other, e.g., with respect to the form of the profile and the positions of peaks and valleys, etc. In other words, the distribution of the water molecules in the direction perpendicular to wall is approximately the same in both cases. However, more water molecules are absorbed on the walls in the case of the L-J potential than the WCAL potential. This is due to the influence of the attractive part of the potential, which increases absorbability of the water molecules.

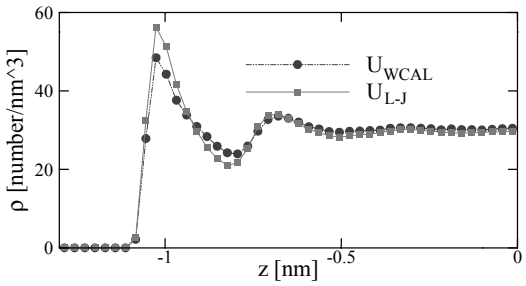

Fig. 3. The number density of oxygen across the channel.

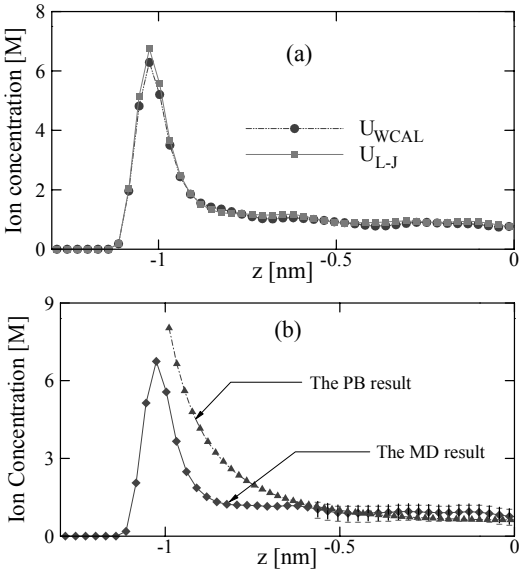

Fig. 4. The ion concentration across the channel: (a) comparison between the result from the WCAL potential and that from the L-J potential and (b) comparison between the PB and MD results with the L-J potential.

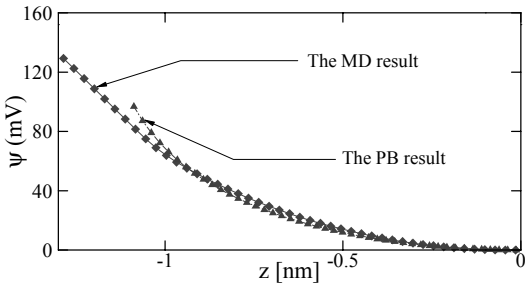

Fig. 5. The electrostatic potential across the channel for the case of the L-J potential.

Fig. 4 shows the ion concentration distributions across the channel. The distributions of ions in the channel are nearly the same for both the WCAL and L-J potentials, as shown in Fig. 4(a). This implies that the influence of the attractive part of the potential on the distribution of the ions is also negligible. In addition, we computed the ion concentration across the channel by using Eq. (9) for comparison, as shown in Fig. 4(b). The solution of the P-B equation is obtained by assuming that

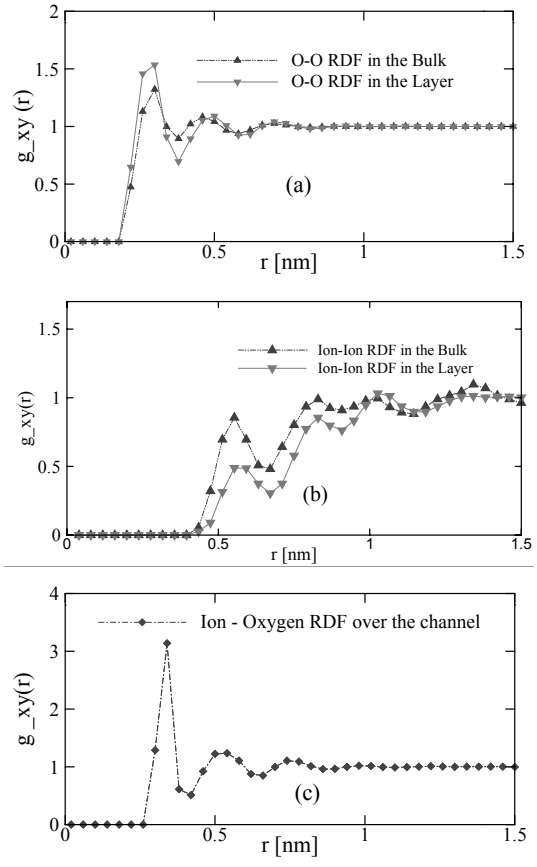

Fig. 6. Distributions of (a) O-O RDFs in the layer and bulk regions, (b) ion-ion RDFs in the layer and bulk regions, and (c) ion-oxygen RDF over the channel (including the layer and bulk regions). These results are obtained with the L-J potential.

the position of the wall, z_{wall}, coincides with the position of the first peak of the ion concentration profile provided by the MD simulation (see Fig. 4(a)) and that the permittivity of the water is constant over the channel [15, 16, 21].

We see that far away from the walls, the P-B solution and the MD result are approximately the same. However, they differ from each other significantly in the region close to the walls. The discrepancy observed in this plot implies that the continuum theory may not hold in this case.

Fig. 5 shows the electrostatic potential across the channel. Here, the P-B solution is obtained from Eq. (8) and the MD result is obtained by numerically solving the Poisson equation (Eq. (1)) with the ion density given from the MD simulation; we assumed a constant permittivity over the channel. It is shown that far away from the walls, the P-B and MD solutions are nearly the same, but they differ from each other in the region near to the walls. The difference between the P-B and MD results can be understood by the significant discrepancy in the ion density distributions in this region, as shown in Fig. 4(b). We notice that P-B curve is steeper than the MD in the region close to the wall. This is contrary to that provided by Kim *et al* [16]. This contradiction is attributed to the difference in the permittivity between our and Kim *et al*.'s cases [16]. We used a constant permittivity of the water in the entire channel, whereas they used a variable permittivity given from the MD simulation. They found that the permittivity is largely changed in the region adjacent to walls.

4.2 Radial distribution functions

In the previous section, we saw that the effect of the attractive part of the potential on the distributions of solvent and the ion across the channel is insignificant almost over the whole region except for in the region near to the wall. In this section, we present the radial distribution function (RDF), in the plane parallel to the wall surface, to further understand this effect on the distributions of the solvent and the ion. The RDF in the *x-y* plane is given as:

$$g_{x-y}(r)=\frac{1}{\rho N\delta V}\left\langle\sum_{i\neq j}\delta\left(\left|r-r_{ij}\right|;\delta r\right)\delta\left(\left|z_j-z_i\right|;\delta z\right)\right\rangle \tag{19}$$

where the function $\delta(|x|;\delta x)$ means:

$$\delta\left(|x|;\delta x\right)=\begin{cases}1 & \text{if } |x|<\delta x/2\\ 0 & \text{else}\end{cases} \tag{20}$$

Further ρ is the density, r_{ij} is the distance measured on the *x-y* plane between the molecules *i* and *j*, and $\delta V=2\pi r\,\delta r\,\delta z$. The product $\delta\left(\left|r-r_{ij}\right|;\delta r\right)\times\delta\left(\left|z_j-z_i\right|;\delta z\right)$ restricts the sum to a pair of atoms located in the same slab of width separated in horizontal range $[r-\delta r/2, r+\delta r/2]$. The physical interpretation of $g_{x-y}(r)$ is that $g_{x-y}(r)\delta V$ is proportional to the probability of finding a molecule in a slab parallel to the walls of thickness δz at a horizontal distance *r*. In a bulk, this would be identical to $g(r)$, the standard RDF.

As shown in the literature (e.g., [19, 20]), the RDF is dependent upon the density, whereas the density varies with z coordinate (Figs. 3 and 4). Hence we first computed the RDFs of ion-ion and oxygen-oxygen in two regions (the first region is the wall layer within 0.4 nm distance from the walls, and the other is the bulk within $-0.7\text{nm}\le z\le 0.7\text{nm}$) for the case of the L-J potential. However, in this paper we will call the wall layer simply the 'layer region'.

Fig. 6 shows RDFs for the oxygen-oxygen (Fig. 6(a)) and ion-ion (Fig. 6(b)) in two different regions. Fig. 6(a) shows two interesting features: first, the first peak of the oxygen-oxygen RDF in the layer region is higher than that in the bulk, and second, two first peaks are located at the same distance $r\approx 0.27\,\text{nm}, 0.47\,\text{nm}$. The value of the first peak reflects the effect of the density on the RDF; in particular, the oxygen atom is more densely packed in the layer region than that in the bulk, and consequently the first peak of the oxygen-oxygen RDF seems to be higher in the layer region. On the other hand, the second observation implies that the position of the peaks is relatively insensitive to the magnitude of the density.

Fig. 6(b) shows ion-ion RDFs with some peculiar as well as

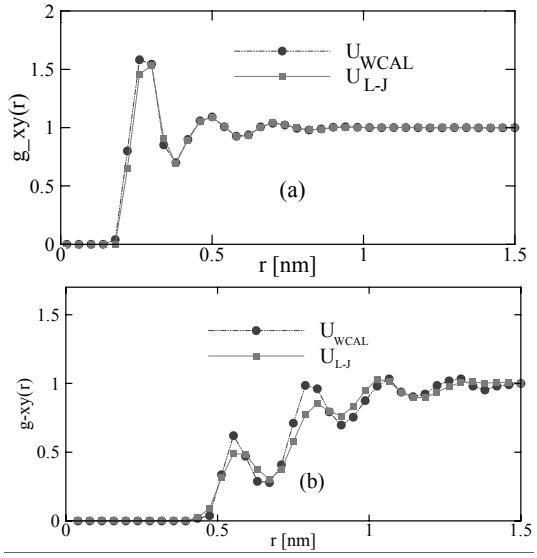

Fig. 7. Comparison of the RDFs in the layer for the cases of the L-J potential and the WCAL potential; (a) O-O RDF and (b) ion-ion RDF.

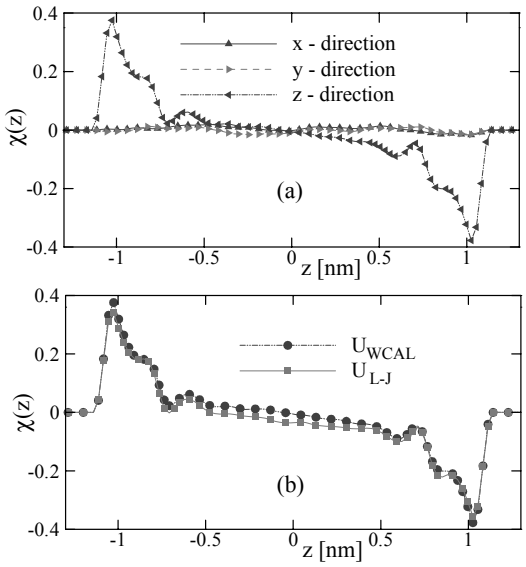

Fig. 8. The averaged projections of the water molecule's dipole moment across the channel: (a) comparison among three components for the case of the L-J potential and (b) comparison of the z-component between the two potentials.

general features. First, the ion-ion RDFs in both regions fluctuate over the entire computational range ($0 < r < 1.5$ nm). In fact, a similar observation for the fluctuation of the ion-ion RDF over the entire computational range was reported by Uchida *et al.* [27] and Lyubartsev *et al.* [28]. In general, presence of peaks in the RDF profiles implies that some local structures (in the statistical sense of course) are expected [19, 20, 27, 28]. The rather persistent fluctuation over the computational range seems to be caused by the effect of water molecules than the ion itself [27, 28]. Next, two first peaks are located nearly at the same distance for both regions. Recalling that the ion density shows a big difference between the layer region and bulk (see Fig. 4(a)), we can say that the density of the ion itself exerts almost no influence on the position of the peaks in the ion-ion RDF. These results are consistent with previous studies [27, 28]. Furthermore, the first peak at 0.5nm is lower than the other peaks particularly in the layer region, which implies that the chloride ions tend to accumulate at the distance 0.5nm but with less probability than the other stable distances, such as 0.8nm or 1.2nm. Such results may be understood by the separation of pairs of the chloride ion due to the water molecules, whose effect should be different for both regions. To confirm that the correlation between the chloride ion and the water molecule is strong, the ion-oxygen RDF is depicted in Fig. 6(c). It is shown that the first peak of the ion-oxygen RDF is quite high, which implies that the distribution of the chloride ions is strongly influenced by the water molecule.

As mentioned in the previous sections, the solution-wall interaction model affects insignificantly the structure of the solution over the channel, except for a slight effect on the layer region. Thus, we compared the RDFs in the layer region to investigate the effect of the solution-wall interaction model. Fig. 7(a) shows that the Oxygen-Oxygen RDFs are nearly the same for both the L-J and WCAL potentials. This may be understood from the fact that the density profiles for both cases are almost the same as shown in Fig. 3. Fig. 7(b) shows again that the ion-ion RDF for different solution-wall interaction potential has only a small difference. Such small difference could be caused by the statistical error. Thus, we can conclude that the effect of the attractive part of the potential on the distributions of the water molecules and the chloride ions, on the plane parallel to the wall surface, is insignificant.

4.3 Profiles of polarization density and dipolar direction of water molecules

In this section, we investigate the effect of the attractive part of the potential on the polarization of water by computing the averaged projection profiles of the dipolar of the water molecules across the channel in both cases. The averaged projection in the n^{th} bin with the number of samples M is defined as [16]:

$$\boldsymbol{\chi}(z_n) = \left\langle \frac{\sum_{i=1}^{N} H_n(z_i)\boldsymbol{\mu}_{water}}{\sum_{i=1}^{N} H_n(z_i)|\mu_{water}|} \right\rangle \tag{21}$$

where $\boldsymbol{\mu}_{water}$ is the dipole moment vector of one water molecule. The physical interpretation of $\boldsymbol{\chi}(z)$ is the averaged vector of the dipolar direction of the water molecule normalized in the n^{th} bin. So, random fluctuation of the orientation (either on the plane or in the space) leads to zero of $\boldsymbol{\chi}$.

Fig. 8(a) shows the averaged projection profiles across the channel for the case of L-J potential. In the x- and y-directions, the averaged projections are approximately equal to zero

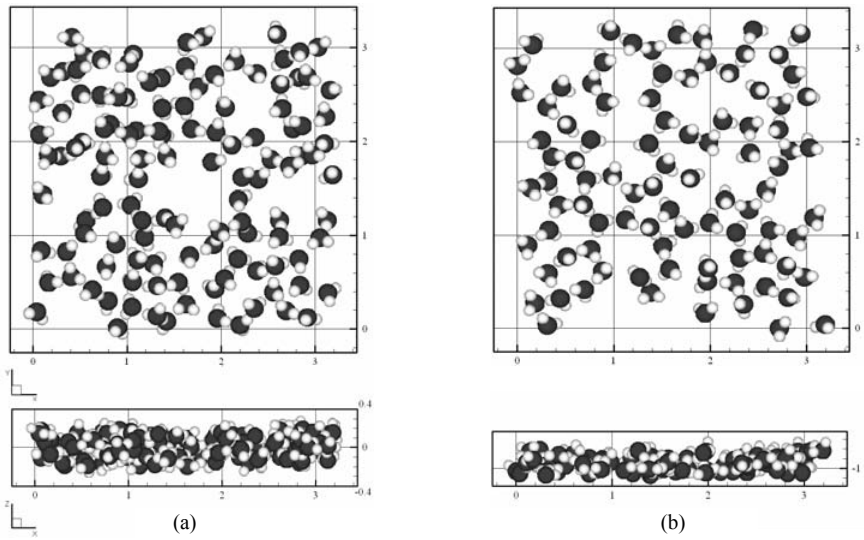

Fig. 9. The snapshots of the water molecules' scatter obtained from the MD simulation at the time t=0.5 ns showing top (upper) and side (lower) views: (a) bulk and (b) layer regions. The Fig. shows that water molecules in the layer region tend to be oriented in such a way that the oxygen atoms are located closer to the wall than the hydrogen atoms and the water molecules in the layer region are more structured than those in the bulk.

across the channel, which implies that the water molecules are isotropically oriented in these directions. This is due to the absence of the external force in these directions, which leads to the water molecu-les tumbled isotropically and randomly by the thermal rotation on the x-y plane. In the *z*-direction, however, the water molecules are preferably oriented, particularly in the region close to the walls, because of the interaction between the water molecules and the walls. In Fig. 8(a), we also notice that the position at which the water molecules are preferably oriented is to coincide with that of the first peak in the number density profile (see in Fig. 3). In fact, the coincidence of these positions is reported in the previous studies [15, 16]. This is related to the layering phenomenon [15]. Fig. 9 is a snapshot of water-molecule configuration obtained from the MD simulation at time t = 0.5 ns. It is shown that water molecules in the regions close to the walls are more oriented than the bulk. A closer look at the region near to the wall indicates that oxygen atoms tend to be closer to the wall than the hydrogen.

Fig. 8(b) shows the *z*-component of the vector $\chi(z)$ obtained from the MD simulations in both potentials. It is shown that profiles are nearly the same in the entire channel. This means that the effect of the attractive part of the potential on the polarization of the water molecules is also weak. This result can be understood as follows: since the oxygen atom is positioned much closer to the mass center of the water molecule and deviation of the forces in the WCAL and L-J potentials resulting from the attractive part remains small, this then leads to the fact that the torque rotating the water molecule is varied insignificantly with the different potential model.

4.4 Dynamic property

Up to now, we have addressed the effect of the attractive part of the potential on the static property of the water molecule and the chloride ion. We found that the static property of the water molecule and the chloride ion is weakly dependent on the attractive part of the potential. In this section, we consider the effect of the attractive part of the solution-wall interaction on the dynamic property of the water molecule on the layer region. The dynamic property is determined by computing the velocity autocorrelation function (VACF) of the translational and rotational motions and the diffusion coefficient. The VACF for the translational motion is defined as:

$$c_v(t) = \langle v(t)v(0)\rangle = \left\langle \frac{1}{N}\sum_{i=1}^{N} v_i(0)v_i(t)\right\rangle \tag{22}$$

where the ensemble average is taken over the number of time origins M_0. The diffusion coefficient is obtained from the VACF by using the following formula:

$$D = \frac{1}{d}\int_0^\infty c_v(t)dt \tag{23}$$

where d takes 1 when diffusion is considered along the z-direction, while it takes 2 for diffusion on the $x-y$ plane. The VACF for the rotational motion can be obtained by using a similar equation to Eq. (22) (but $v(t)$ must be replaced by $\omega(t)$ the Z-component of the angular velocity vector $\boldsymbol{\omega}$ referred to the body-fixed coordinate for the water, as shown in Fig. 1(b)).

Fig. 10 shows VACFs for the translational motion in the *z*-direction (Fig. 10(a)) and those for the rotational motion (Fig. 10b); the VACFs shown in this Fig. are normalized by the value at t = 0. We estimated the errors of the VACFs to be less than 0.5% with 95% confidence. We see that the translational VACF decays more slowly than the rotational VACF, similar to Lyubartsev *et al* [28]. The reason for this result can be explained by using an order of analysis from the thermal motion

Table 2. The diffusion coefficient of the water molecules in the layer region.

	$D_{x\text{-}y}(10^{-9}m^2/s)$	$D_z(10^{-9}m^2/s)$
WCAL potential	2.93	2.28
L-J potential	2.68	2.02

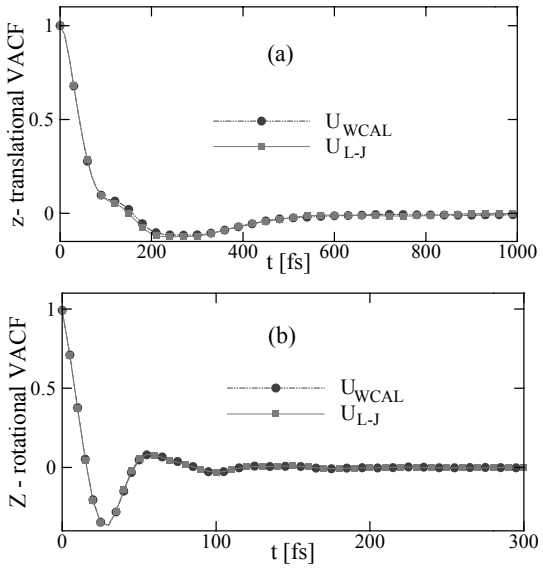

Fig. 10. Comparison of (a) the translational and (b) rotational VACFs of the water molecules between the WCAL and L-J potentials in the layer region.

and Newton's equation of motion. From Newton's equations for the water molecule's translational and rotational motions, we have $bdv/dt \sim \varepsilon^2 d\omega/dt$ where b is the distance between the oxygen and the hydrogen and ε is the distance between the oxygen and the center of mass. On the other hand, from the thermal motion, we have $v \sim \varepsilon\omega$. Combining these two results we get the final result $t_v/t_\omega \sim b/\varepsilon >> 1$ where time scales for each motion read $t_v \sim v/(dv/dt)$ and $t_\omega \sim \omega/(d\omega/dt)$. Fig. 10 also shows that the z-direction VACFs for the rotational motion are virtually the same for both L-J and WCAL potentials. On the other hand, the z-direction VACF for the translational motion for the WCAL potential is slightly higher than that for the L-J potential in the time range, $100\text{ fs} < t < 200\text{ fs}$, which leads to the result that the diffusion coefficient for the WCAL potential is accordingly higher than that for the L-J potential.

Table 2 shows the diffusion coefficients of the water molecules in the region from -1.3nm to -0.9nm nm for both cases, which are obtained by using the VACF, i.e., Eq. (23). The errors of diffusion coefficients were estimated to be less than 3% with 95% confidence. Two interesting features can be seen from this table. First, the diffusion coefficient of the *z*-component is less than that of the *x-y* component in each case.

This is understood as the motions of the water molecules in the *z*-direction are strongly restricted by the presence of the walls. Second, the diffusion coefficient for the case of the WCAL potential is larger than that for the other. The result means that the water molecules are more mobilized with the WCAL potential than with the L-J potential. This can be explained by the fact that the water density in the case of the L-J potential is larger [19, 20], as shown in Fig. 3.

5. Conclusions

Using the MD simulations, we have addressed the effect of the water-wall and ion-wall interaction potentials on the properties of chloride solutions confined within the uniformly charged plates. Based on discussions and the numerical results, the following conclusions can be drawn.

(1) The static property of the solvent and ion is weakly dependent on the attractive part of the solution-wall interaction potentials, except for the water and ion distributions in which more water molecules are absorbed on the walls for the case of the L-J potential than for the case of the WCAL potential.

(2) We compared the MD results with the P-B solutions. Far away from the channel wall, the key physical values such as the ion concentration and the electrostatic potential obtained by both methods are in good agreement with each other. However, agreement cannot be attained in the region close to the walls. This implies that for the nano-scale system the continuum model may not work at least in the region close to the walls.

(3) We computed the VACFs and derived the diffusion coefficients of the water molecules, in the region close to the walls, to understand the effect of the wall-water and water-ion interactions on the dynamic property of the water molecules. In this region, the water molecules show higher diffusion coefficients with the WCAL potential than the L-J potential.

Acknowledgments

This work was supported by the National Research Foundation of Korea (NRF) through the National Research Laboratory Program funded by the Ministry of Science, Education and Technology (No. 2005-1091). This work was also supported by NRF grant No.2009-0083510 through Multi-phenomena CFD Engineering Research Center.

References

[1] L. Joly, C. Ybert, E. Trizac and L. Bocquet, Liquid friction charged surfaces: From hydrodynamic slippage to electrokinetics. *J. Chem. Phys.*, 125, 204716 (2006) 1-14.

[2] L. Joly, C. Ybert. E. Trizac and L. Bocquet, Hydrodynamics within the Electric Double Layer on slipping surface. *Phys. Rev. Lett.*, 93, 257805 (2004) 1-4.

[3] J. L. Barrat and L. Bocquet, Large slip effect at a nonwetting fluid-solid interface. *Phys. Rev. Lett.*, 82 (1999) 4671-4674.

[4] D. M. Huang, C. C. Bizonne, C. Ybert and L. Bocquet, Aqueous electrolytes near hydrophobic surfaces: Dynamic effects of ion specificity and hydrodynamic slip. *Langmuir*, 24 (2008) 1442-1450.

[5] D. M. Huang, C. C. Bizonne, C. Ybert and L. Bocquet, Ion-specific anomalous electrokinetic effects in hydrophobic nanochannels. *Phys. Rev. Lett.*, 98, 177801 (2007) 1-4.

[6] D. M. Heyes and H. Okumura, Equation of state and structural properties of the Weeks-Chandler-Andersen fluid. *J. Chem. Phys.*, 124, 164507 (2006) 1-8.

[7] S. P. Tan, D. Adidharma and M. Radosz, Weeks-chandler-andersen model for solid-liquid equilibria in lennard-jones systems. *J. Phys. Chem. B*, 106 (2002) 7878-7881.

[8] K. P. Travis and K. E. Gubbins, Poiseuille flow of Lennard-Jones fluids in narrow slit pores. *J. Chem. Phys.*, 112 (2000) 1984-1994.

[9] P. Kumar, F. W. Starr, S. V. Buldyrev and H. E. Stanley, Effect of water-wall interaction potential on the properties of nanoconfined water. *Phys. Rev. E*. 75, 011202 (2007) 1-8.

[10] P. Kumar, S. V. Buldyrev, F. W. Starr, N. Giovambattista and H. E. Stanley, Thermodynamics, structure, and dynamics of water confined between hydrophobic plates. *Phys. Rev. E*. 72, 051503 (2005) 1-12.

[11] S. H. Lee and P. J. Rossky, A comparison of the surface and dynamics of liquid water at hydrophobic and hydrophilic surfaces – a molecular dynamics simulation study. *J. Chem. Phys.*, 100 (1993) 3334-3345.

[12] C. T. Lee, J. A. MacCammon and P. J. Rossky, The structure of liquid water at an extended hydrophobic surface, *J. Chem. Phys.*, 80 (1984) 4448-4455.

[13] L. N. Glosli and M. R. Philpott, olecular dynamics study of interfacial electric fields, *Electrochimica Acta*, 41 (1996) 2145-2158.

[14] S. B. Zhu, M. R. Philpott and J. N. Glosli, Comparison of water models in simple electric double layers, *Storming Media*, Pentagon Rep. No. A110482 (1994).

[15] J. B. Freund, Electroosmosis in a nanometer-scale channel studied by atomistic simulation, *J. Chem. Phys.*, 116 (2001) 2194-2200.

[16] D. Kim and E. Darve, Molecular dynamics simulation of electroosmotic flow in rough wall nanochannels, *Phys. Rev. E*, 73, 051203 (2006) 1-12 and High-ionic-strength electroosmotic flows in uncharged hydrophobic nanochannels, J. Colloid and Interface Sci., 330 (2009) 194-200.

[17] W. H. Press, S. A. Teukolsky, W. T. Vetterling and B. P. Flannery, *Numerical Recipes in the Fortran*, 2nd edition, Cambridge University Press (1992).

[18] http://www.lsbu.ac.uk/water/models.html

[19] M. P. Allen and D. J. Tildesley, *Computer Simulation of Liquids*, Clarendon Press, Oxford (1987).

[20] D. C. Rapaport, *The Art of Molecular Dynamics Simulations*, Cambridge (2002).

[21] R. Qiao and N. R. Alura, Ion concentrations and velocity profiles in nanochannel electroomostic flows. *J. Chem. Phys.*, 118 (2002) 4692-4701.

[22] I. C. Yeh and M. L. Berkowitz, Ewald summation for systems with slab geometry, *J. Chem. Phys.,* 111 (1999) 3155.

[23] W. Yang, X. Jin and Q. Liao, Ewald summation for uniformly charged surface, *J. Chem. Theory Comput.*, 2 (2006) 1618-1623.

[24] M. Deserno and C. Holm, How to mesh up Ewald sums. II. An accurate error estimate for the particle–particle–particle-mesh algorithm, *J. Chem. Phys.*, 109 (1998)7694-7701.

[25] H. Hoang, S. Kang and Y. K. Suh, Molecular-dynamic simulation on the statical and dynamical properties of fluids in a nano-channel, *J. Comput. Fluids Eng.*, 13 (4), (2009) 24-34.

[26] Help of MATLAB 7.0.

[27] H. Uchida and M. Matsuoka, Molecular dynamics simulation of solution structure and dynamics of aqueous sodium chloride solutions from dilute to supersaturated concentration, *Fluid Phase Equilibria*, 219 (2003) 49-54.

[28] A. P. Lyubartsev and A. Laaksonen, Concentration Effects in Aqueous NaCl Solutions. A Molecular Dynamics Simulation, *J. Phys. Chem.,* 100 (1996) 16410-16418.

Hai Hoang received his B.S. degree in 2007 from the Aeronautical Engineering Department, Ho Chi Minh City University of Technology, Vietnam. He then received his M.S. degree in 2009 from the Department of Mechanical Engineering, Dong-A University, Busan, Korea. Now, he is working as a Ph. D student in multi-scale fluid flows at Laboratoire des Fluides Complexes in France.

Sangmo Kang received B.S. and M.S. degrees from Seoul National University in 1985 and 1987, respectively, and then worked for five years in Daewoo Heavy Industries as a field engineer. He also achieved a Ph.D. in Mechanical Engineering from the University of Michigan in 1996. Dr. Kang is currently a Professor at the Department of Mechanical Engineering, Dong-A University in Busan, Korea. His research interests are in the area of micro- and nanofluidics and turbulent flow combined with the computational fluid dynamics.

Yong Kweon Suh received his B.S. degree in 1974 from the Department of Mechanical Engineering, Seoul National University, Korea, and his M.S. and Ph. D degrees from State University of New York at Buffalo, USA, in 1985 and 1986, respectively. Since 1986, he has been working at the Department of Mechanical Engineering, Dong-A University, Busan, Korea.